Journal of Systems Engineering and Electronics
Vol. 28, No. 3, June 2017, pp.597 – 605

Image haze removal via multiscale fusion and total variation

Xuemei Wang[1], Mingye Ju[2], and Dengyin Zhang[2,*]

1. School of Computer Science, Nanjing University of Posts and Telecommunications, Nanjing 210003, China;
2. School of Internet of Things, Nanjing University of Posts and Telecommunications, Nanjing 210003, China

Abstract: In foggy weather, images of outdoor scene are usually characterized with poor visibility as well as faint color saturation. The degraded hazy images may have substantial negative impact on most computer vision systems. Thus image haze removal is of the practical significance in engineering. This paper proposes a fast and effective single image haze removal algorithm on the basis of the physics imaging model. To extract the global atmospheric light accurately, we exploit multiple prior rules underlying hazy images, and put forward a novel measurement to judge the likelihood that a pixel is regarded as the global atmospheric light. In addition, the rough transmission map is estimated through a multiscale fusion process based on the Laplace pyramid transform, and refined by a total variation model. Experimental results demonstrate the proposed method outperforms most of the state-of-the-art algorithms in terms of the dehazing quality, and achieves a trade-off between the computational efficiency and haze removal capability.

Keywords: multiscale fusion, total variation, multiple prior, transmission refinement.

DOI: 10.21629/JSEE.2017.03.19

1. Introduction

Outdoor images captured in foggy weather usually degrade in color, texture, and contrast. Effective automatic haze removal techniques aim at restoring the scene radiance and will benefit many computer vision applications. Due to the dependence of hazy image degradation on the scene depth, traditional techniques of image processing [1, 2] are inadequate in haze removal.

In recent years, it has caught great attention to haze removal on the basis of the atmospheric scattering model, in which it is critical to estimate the scene depth. Kopf et al. [3] constructed the scene depth map from the corresponding known 3D model. In [4, 5], multiple images taken with different degrees of polarization or under different weather conditions were used to derive the scene depth. Since the requirements are usually hard to be fulfilled, these methods [4, 5] are restrictive in most practical applications.

It becomes more challenging to remove haze from one single hazy image. Hence most existing endeavors are devoted to finding valuable prior knowledge or constraints, which are helpful in image haze removal. Among them, He et al. [6] discovered the dark channel prior (DCP), that most local patches contain some pixels with very low intensity in at least one color channel, and applied DCP in haze removal, producing the compelling results. However, the method [6] is prohibitive in real-time applications owing to the intensive computational overhead introduced by the soft matting operation in transmission refinement.

Subsequently, quite a few algorithms were proposed on the basis of DCP, in which the haze removal process was indeed accelerated. For instance, in [7], the guided filter was employed to speed up the transmission refinement. Because of the guidance of the original color hazy image, the restored image preserves the edge sharpness consistent to the hazy input. Tarel et al. [8] used the median filter to estimate the dissipation function, leading to better efficiency. Since the median filter is not good at edge preserving, a small amount of mist would remain around the depth jumps of scene. Meng et al. [9] adopted a regularization model to blur the transmission map, which was estimated by exploiting the inherent boundary constraint. In the resultant images, the color fidelity is prone to distortion when dealing with white objects. Zhang et al. [10] executed the parallel processing through the graphic processing unit (GPU) and 80 frames could be recovered per second.

As far as the estimation on the global atmosphere light is concerned, many efforts have been devoted to increasing its accuracy. Tan et al. [11] selected the maximum pixel intensity as the global atmospheric light. In [6], the top 0.1% pixels were selected from the dark channel map, and the

Manuscript received June 12, 2016.
*Corresponding author.
This work was supported by the National Natural Science Foundation of China (61571241), the Industry-University-research Prospective Joint Project of Jiangsu Province (BY2014014), the Major Projects of Jiangsu Province University Natural Science Research (15KJA510002), the Jiangsu Province Graduate Research and Innovation Project (CXZZ130476), and the Science Research Fund of NUPT (NY215169).

brightest one was treated as the global atmospheric light. Kim et al. [12] proposed a scoring mechanism to determine the candidate patch, from which the global atmospheric light was extracted. These methods [6,11,12] all failed to deal with bright scene objects.

In this paper, we propose a DCP based method, which proves to be fast and effective in removing haze from one single outdoor image. The main contributions of this method include: (i) Multiple priors are exploited to design a novel measurement in estimating the global atmospheric light; (ii) Laplace pyramid (LP) fusion process is employed to estimate the transmission map, and the total variation (TV) model is adopted in further transmission refinement. The experimental results demonstrate that our method is competitive in both visual quality and efficiency.

The rest of the paper is organized as follows. We firstly briefly review the fundamental DCP based algorithm of haze removal in Section 2. In Section 3, our method of estimating the global atmospheric light is provided. In Section 4, the transmission calculation via multiscale LP fusion and TV model is presented. Section 5 shows our experimental results in both qualitative and quantitative ways. Finally, we conclude the paper in Section 6.

2. Related work

2.1 Physical imaging model

In computer vision and graphics, the atmospheric scattering model can be described as

$$I(x) = J(x)t(x) + A(1 - t(x)) \tag{1}$$

where I is the observed image, J is the scene radiance, A is the global atmospheric light and usually assumed as a constant, $t(x)$ denotes the transmission coefficient. As the physical imaging model in (1) states, the image degradation originates from two aspects. One is the direct attenuation, in which the scene radiance is decayed in the transmission medium, while the other is the additive ambient light that comes from the scattering behavior by atmospheric aerosols. The goal of the haze removal is to recover J from I.

2.2 Dark channel prior based dehazing

The fundamental procedure of the DCP based haze removal consists of three steps [6]. Firstly, the global atmospheric light A is extracted from the hazy input. Then the block-min operation is performed on the input I to obtain the corresponding dark channel.

$$I^{\mathrm{dark}}(x) = \min_{y\in\Omega(x)} \min_{c\in\{\mathrm{R,G,B}\}} I^c(y) =$$

$$t(x) \min_{y\in\Omega(x)} \min_{c\in\{\mathrm{R,G,B}\}} J^c(y) + A(1 - t(x)). \tag{2}$$

From the DCP rule, we have

$$\min_{y\in\Omega(x)} \min_{c\in\{\mathrm{R,G,B}\}} J^c(y) \to 0. \tag{3}$$

Thus, the transmission can be derived by

$$t = 1 - \frac{I^{\mathrm{dark}}}{A}. \tag{4}$$

To make the restored image seem more natural, (4) can be rewritten as

$$t = 1 - \omega\frac{I^{\mathrm{dark}}}{A} \tag{5}$$

where the constant ω $(0 < \omega \leqslant 1)$ is introduced to keep a very small amount of haze for distant objects.

Finally, the scene radiance is recovered by

$$J(x) = \frac{I(x) - A}{\max(t(x), t_0)} + A \tag{6}$$

where t_0 represents the lower bound of the transmission.

3. Multi-prior estimation on the global atmospheric light

Most existing methods fail to deal with white objects in extracting the global atmospheric light. The brightness or dark channel may not suffice in estimation. Through observations on a large amount of hazy images, we find that heavy haze regions exhibit local smoothness besides high brightness. That means, neighboring pixels in dense foggy or sky areas are closer in intensity. Fig. 1(b) and Fig. 1(c) show the brightness map and the normalized mean gradient map after smoothed processing on Fig. 1(a). Clearly, regions of heavy haze or sky seem dark on the whole in the gradient map. Here, we refer this observation as the luminance smoothness prior in heavy hazy regions.

Also in foggy or sky areas, the color of pixels is most distributed around the diagonal line in a RGB cube range. To make it clear, we define the color channel variance [13] as

$$S = \sqrt{(I^{\mathrm{R}} - L)^2 + (I^{\mathrm{G}} - L)^2 + (I^{\mathrm{B}} - L)^2} \tag{7}$$

where L is the gray image computed by

$$L = \frac{1}{3}\sum_{c\in\{\mathrm{R,G,B}\}} I^c \tag{8}$$

where $I^c (c \in \{\mathrm{R, G, B}\})$ denotes the RGB color component. It can be inferred from (7) that the larger value of S indicates higher purity in color. Fig. 1(d) shows the image S calculated from Fig. 1(a). As can be seen clearly, the color channel variance tends to be zero for pixels in the distant foggy sky regions. We refer this discovery as the color saturation prior found in thick foggy regions.

Combined with the priors on brightness, smoothness and color, we come up with a quantitative measurement in

(9) to evaluate the likelihood that a pixel should be selected as the global atmospheric light.

$$F(x,y) = \exp\left(-\frac{(L(x,y)-1)^2}{2\sigma_1^2}\right)\cdot$$

$$\exp\left(-\frac{(-\nabla L(x,y))^2}{2\sigma_2^2}\right)\exp\left(-\frac{(-S(x,y))^2}{2\sigma_3^2}\right) \qquad (9)$$

where σ_1, σ_2, σ_3 are scales in the three exponential terms ($\sigma_1 = 0.3$, $\sigma_2 = 0.1$, $\sigma_3 = 0.1$), S denotes the color variance defined in (7), ∇L refers to the L's gradient calculated by

$$\nabla L(x,y) = \sqrt{(\nabla_x L(x,y))^2 + (\nabla_y L(x,y))^2} \qquad (10)$$

where

$$\begin{cases} \nabla_x L(x,y) = L(x+1,y) - L(x,y) \\ \nabla_y L(x,y) = L(x,y+1) - L(x,y) \end{cases}. \qquad (11)$$

Before computing $F(x,y)$, all the three quantities $(L(x,y), \nabla L(x,y), S(x,y))$ need to be processed by mean filtering (the template size is 20×20 in our experiments).

(a) Hazy image (b) Brightness map

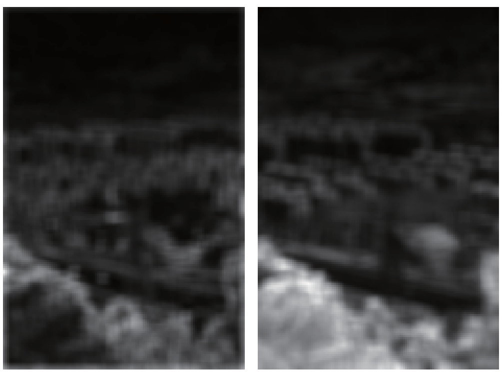

(c) Gradient map (d) Variogram

(e) The 1st term in (9) (f) The 2nd term in (9)

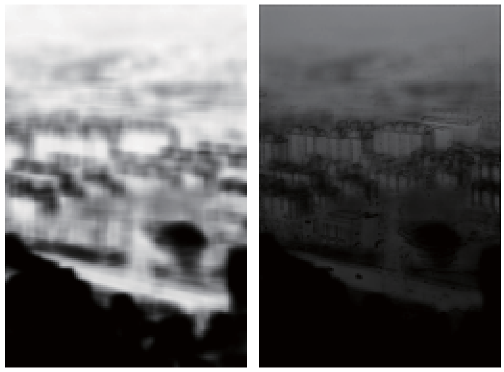

(g) The 3rd term in (9) (h) The resultant F

Fig. 1 Images derived from the input hazy image

In (9), the first term describes the contribution from the brightness. Apparently, it is close to one when the pixel brightness approaches one. If only the first term is considered, the brighter pixel is more likely to be selected as the global atmospheric light. The second term evaluates the importance of local smoothness. The small gradient indicates low contrast and the high similarity in intensity among neighbor pixels. And this conforms to the local smoothness prior of dense haze or sky regions. The third term takes the impact of color saturation into account, and it approaches one when the difference among three color components is trivial. The detailed procedure to estimate the global atmospheric light A is summarized in Algorithm 1.

Algorithm 1 Estimation on A

Input Hazy image I

Output Global atmospheric light A

Step 1 Produce three images $(L, \nabla L, S)$ by (8), (10) and (7) respectively, and smooth them by the mean filtering.

Step 2 Calculate $F(x,y)$ for each pixel (x,y) by (9).

Step 3 Rank F in a decreasing order, and find the pixel (x^*, y^*) with maximum F. $L(x^*, y^*)$ is set as the expected output A.

Fig. 2(a) marks the positions selected as the atmospheric light by Namer [14], He [6], Kim [12] and our method. As shown in Fig. 2(a), both Namer [14] and He [6] treat the bright pixel on two different umbrellas as the atmospheric light. Kim [12] succeeds in recognizing the right region thick haze hangs over. Unfortunately, the white text on the license plate of a car resides in the identified region, which causes the unexpected estimation deviation. In contrast, our proposed method is able to extract the atmospheric light accurately. Fig. 2(b) – Fig. 2(e) show the restored results from [14], [6], [12] and our method. As can be seen, our proposed method exhibits more compelling effect in visibility.

(a) Estimation on the atmospheric light

(b) Result by Namer [14]

(c) Result by He [6]

(d) Result by Kim [12]

(e) Result by the proposed method

Fig. 2 Comparison of the atmospheric light estimation and the resultant dehazing effect

4. Transmission refinement

For an ideal transmission map, two kinds of local regularization must be considered. One is the local dependency. Since the change in scene depth is gradual in most cases, the transmission in a local region can be assumed to be constant. Thus, to achieve the satisfactory visual quality, the local smoothness is a critical constraint on transmission. On the other hand, to prevent from halo effects, it is also important to preserve the abrupt depth discontinuities and outline the profile of the foreground objects. Hence, our major goal in transmission refinement is to attain local smoothness while preserve abrupt depth jumps.

The transmission directly calculated from the DCP rule inevitably has block effects, leading to halo artifacts around the depth jumps in the restored results. Here, we intend to produce the transmission map equipped with the required features. Firstly, two coarse transmission maps are derived from the dark channels by (2). One dark channel is generated in a pixel wise manner, in which the min operation is applied pixel by pixel to obtain the minimum in the RGB space. We refer the transmission map derived from this pixel-based dark channel map (PDCM) as pixel-based transmission map (PTM). The other dark channel is resulted from patch based filtering, in which the spatial correlation of image pixels is exploited and the erosion operation is employed on the PDCM. We denote the transmission map derived from the latter dark channel as a block-based transmission map (BTM). Fig. 3(a) and Fig. 3(b) show the BTM and PTM, respectively. As can be seen clearly, PTM is capable of preserving almost all the details about edge and texture in the input, while BTM tends to blur depth discontinuities. Since the local smoothness is a critical constraint for transmission, the detailed texture structure is not expected in local patches. It is urgent to eliminate texture details within small neighboring regions. Meanwhile, the abrupt depth discontinuities should be attained.

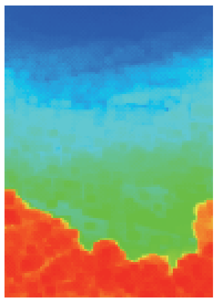

(a) BTM

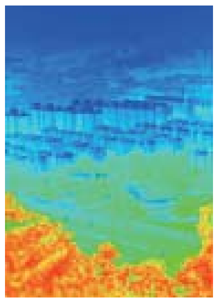

(b) PTM

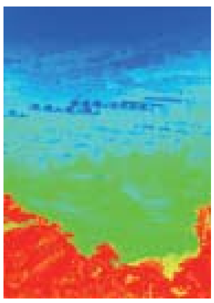

(c) Fusion result

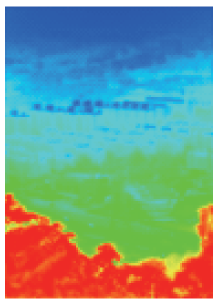

(d) Refined result by TV

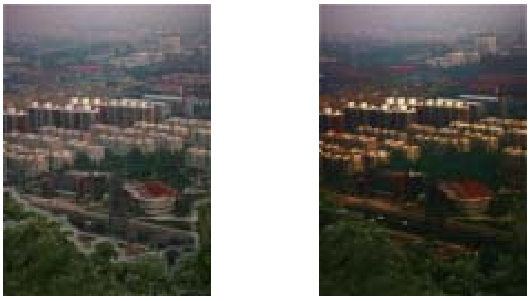

(e) Result from (a) (f) Result from (b)

(g) Result from (c) (h) Result from (d)

Fig. 3 Transmission refinement by fusion and TV

Next, a fusion process is implemented to estimate the transmission by combining positive features from PTM and BTM. In order to extract valuable information underlying PTM and BTM, we decompose them into several components with various scales by the LP decomposition. As is known, most low frequency information appears in the high-level components, while mid-and-high frequency parts largely reside in the low-level ones. Moreover, the low-level components in PTM and the high-level components in BTM seem more valuable and may contribute more to the ultimate fusion result. For this purpose, we apply a level-dependent fusion strategy on PTM and BTM in each layer:

$$H_i = P_i\left(1-\left(\frac{i}{N}\right)^3\right) + B_i\left(\frac{i}{N}\right)^3 \tag{12}$$

where N is the number of LP levels, $\{P_i\}, \{B_i\}$ $(1 \leqslant i \leqslant N)$ denote the LP decomposition results from PTM and BTM respectively, H_i $(1 \leqslant i \leqslant N)$ is the fusion result of each layer. In (12), H_i can be regarded as a linear combination of P_i and B_i. Since the important edge details are mainly contributed by the low-level P_i, the weight of P_i decreases along with i. Likewise, the high-level B_i contains more valuable smooth components, so the weight of B_i increases along with i.

Once the fusion operation is accomplished in each level, the LP reconstruction process can be carried out to form the transmission map of original size. Fig. 3(c) gives the fusion result. Apparently, the fusion map inherits most depth discontinuities from Fig. 3(b), and the block effect is almost eliminated. However, it can also be observed that some texture noise still exits in the fusion result. Due to the irrelevance to scene depth, texture details in transmission will have undesirable effects on the restored result. Thus it is necessary to make a further improvement on the transmission. Here, we propose a total variation optimization model for refinement:

$$\arg\min_t E = \frac{\lambda}{2}\|t-\widehat{t}\|^2 + \frac{1}{2}\|W\nabla t\|^2 \tag{13}$$

where $\widehat{t}$ denotes the transmission produced by the fusion process, t denotes the refined transmission, λ is the regularization parameter for balancing the two terms ($\lambda = 3$ in our experiment). In (13), the first term is to measure the fidelity of t to $\widehat{t}$, and the second term is to ensure the local dependency constraint on transmission. W is a weighting function defined as

$$W(x,y) = \mathrm{e}^{-\frac{\|\nabla L(x,y)\|_2^2}{2\sigma}} \tag{14}$$

where (x,y) denotes the pixels' position, ∇L is defined in (10), σ is the scaling factor ($\sigma = 0.1$ in our experiment). Clearly, the weight W varies inversely with the brightness gradient. It makes sense that pixels within smooth regions are likely to be assigned large weights while those near or on the edges have small weights. By solving (13), we can find an optimal transmission map, which ensures the local smoothness and prevents from blurring the important edge details simultaneously.

To speed up the solving process, we adopt the gradient approximation method [15], in which ∇t is replaced with

$$\nabla t(x,y) = \frac{1}{r^2-1}\sum_{i=1}^{r^2-1}(t(x,y)-t_i(x,y)) \tag{15}$$

where r is the size of neighborhood, t_i is the transmission of the ith pixel in a local patch centered at (x,y). That is to say, the gradient is calculated approximately by averaging all the first order difference between the pixel and its neighbors.

For convenience, a fast iterative procedure is designed to find the solution in (13). For each current iteration, t_i is expressed approximately as the outcome t from the last iteration. To find the result of $t^{(j)}$ in the jth iteration, we need to calculate the partial derivative of E with respect to $t^{(j)}$ and make it equal to zero.

$$\frac{\partial E}{\partial t^{(j)}} = \lambda(t^{(j)} - \widehat{t}) + W\sum_{i=1}^{r^2-1}(t^{(j)} - t_i^{(j-1)}) = 0 \tag{16}$$

Then

$$t^{(j)} = \frac{\lambda\widehat{t} + W\sum\limits_{i=1}^{r^2-1} t_i^{(j-1)}}{\lambda + W(r^2-1)}. \tag{17}$$

Fig. 3(d) shows the transmission map after TV optimization. Compared with Fig. 3(c), some tiny texture details irrelevant to depth have been blurred furthermore. Accordingly, the quality of haze removal has been improved as shown in Fig. 3(h).

5. Experimental results

To demonstrate the effectiveness of our proposed method, we compare our approach with some up-to-date algorithms in both qualitative and quantitative manners. Those algorithms we select for comparison include He [6], Meng [9], Zhu [16], Tarel [8], and Choi [2]. All the experiments are conducted in MatlabR2012a on a PC with a 2.5 GHz Intel Core (TM) i5-3210M CPU. We test the performance of all the algorithms on several benchmark hazy images, which exhibit diverse challenges in haze removal. The parameters used in our method are set as follows: the patch size used in BTM is 15, and the level number of LP decomposition is 7. In (15), $r = 13$. Other parameters have been mentioned in Sections 3 and 4. For the sake of fairness, we run those algorithms [2,6,8,9,16] with the parameters recommended by the authors .

5.1 Qualitative comparison

Fig. 4 shows the restored results from our proposed method. There are seven test images in Fig. 4: from left to right, "Test1", "Test2", "Test3", "Test4", "Test5", "Test6" and "Test7", respectively. As can be seen in Fig. 4, our approach works well in removing haze from these test images. For images with distant scenery, such as "Test1", "Test3", "Test5" and "Test7", both the visibility and color fidelity are enhanced significantly. More than that, the clear texture details are restored in "Test2", and nearly none of halo artifacts are found in the regions with frequent abrupt depth jumps in "Test4". Besides, for images captured in very dense haze condition, such as "Test6", the details of scene objects are unveiled and the vivid color information is recovered.

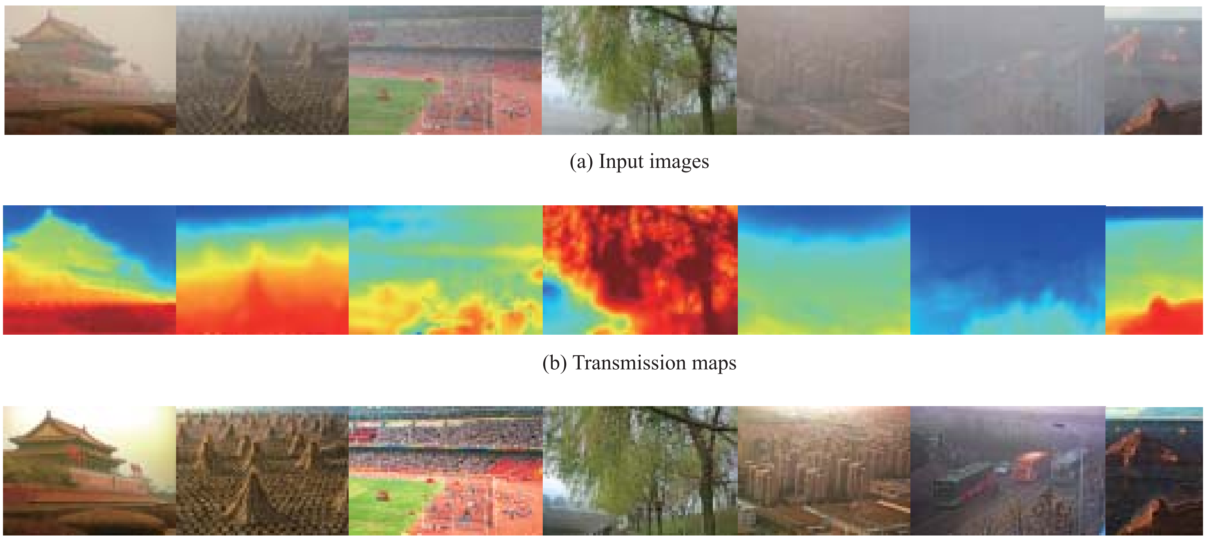

(a) Input images

(b) Transmission maps

(c) Haze removal results

Fig. 4 Test images (1)

Fig. 5 compares our algorithm with several other representative haze removal methods [2,6,8,9,16]. In Fig. 5, from left to right, it displays the input hazy images, the results obtained by He [6], Meng [9], Zhu [16], Tarel [8], Choi [2] and our method respectively.

It can be observed in Tarel's results that most texture details are well restored after haze removal. However, due to the median filter used in estimating the dissipation function, Tarel [8] shows poor performance in removing haze from regions with depth discontinuities. Moreover, its dehazing quality is not satisfactory in case of dense haze.

He's method [6] is able to achieve a compelling visual effect in most cases. Nevertheless, the deviation in the estimate of the global atmospheric light will inevitably cause the degraded contrast in the dehazing results (see Fig. 5(b)). What's more, He's results suffer from severe color distortion if there are scene objects of large size with similar brightness to the airlight (see Fig. 5(e)).

Meng's results are close to He's in haze removal quality. Although the boundary constraint is introduced to estimate the transmission map, Meng [9] shares the same limitation with He [6] in haze removal: the color fidelity is prone to be distorted when dealing with large white objects (see Fig. 5(e)).

Zhu [16] is effective in preventing from excessive haze removal and the results are not over-enhanced (see Fig. 5(e)). Yet, the fixed setting of scattering coefficient usually results in incomplete haze removal (see Fig. 5(a) and Fig. 5(b)).

Different from the algorithms [6,8,9,16], Choi [2] recovered hazy images on the basis of the referenceless perceptual haze density prediction model, rather than the atmospheric scattering model. From Fig.5, we find that the results obtained by Choi [2] are less favorable in terms of both visibility and color fidelity.

In contrast, the results obtained by our method are comparable to or better than that of the other five methods. In particular, the advantages of our method can be fully exhibited in Fig. 5(d) and Fig. 5(e), where the unexpected over-enhancement is not found and the color fidelity is well kept in the outcome.

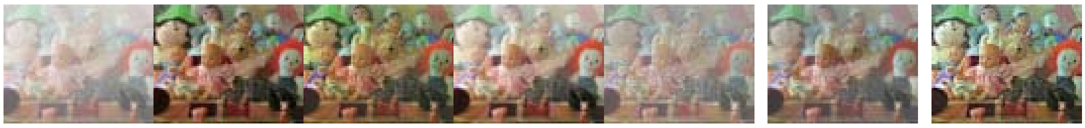

(a) The 1st hazy image and its dehazed results

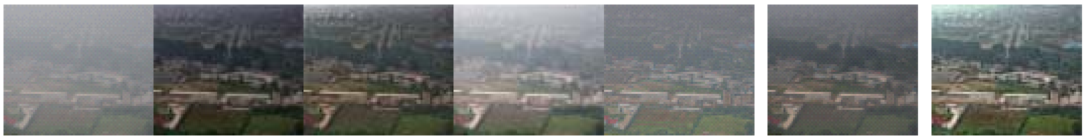

(b) The 2nd hazy image and its dehazed results

(c) The 3rd hazy image and its dehazed results

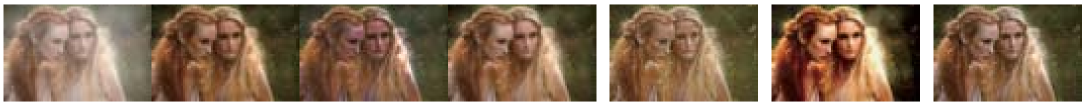

(d) The 4th hazy image and its dehazed results

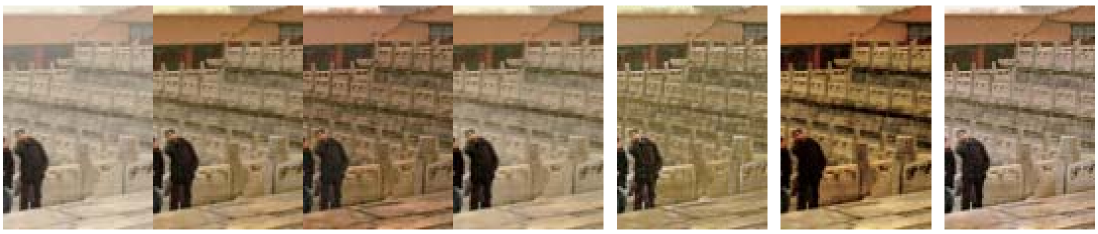

(e) The 5th hazy image and its dehazed results

Fig. 5 Test images (2)

5.2 Quantitative comparison

To quantitatively assess the visual quality after haze removal, we employ three variables (e, r, d). The first two measurements (e and r) are recommended in [17]: i.e. e denotes the rate of edges newly visible, r expresses the quality of contrast restoration. d is defined in [2] to represent the haze density. We calculate these three measurements (e, r, d) from the images in Fig. 5, and show the quantitative comparison results in Fig. 6. It can be seen that, the quantitative results from our method take the first or second place in e and r overall. And the results from He [6] and Meng [9] have little difference with each other. It conforms to the qualitative comparison results shown in Fig. 5. Although Choi [2] has the minimum value in d for the last three images, it does not indicate that it outperforms our algorithm. As can be seen clearly in Fig. 5(d) and Fig. 5(e), the excessive haze removal occurs in Choi's results and the output images are over-enhanced significantly.

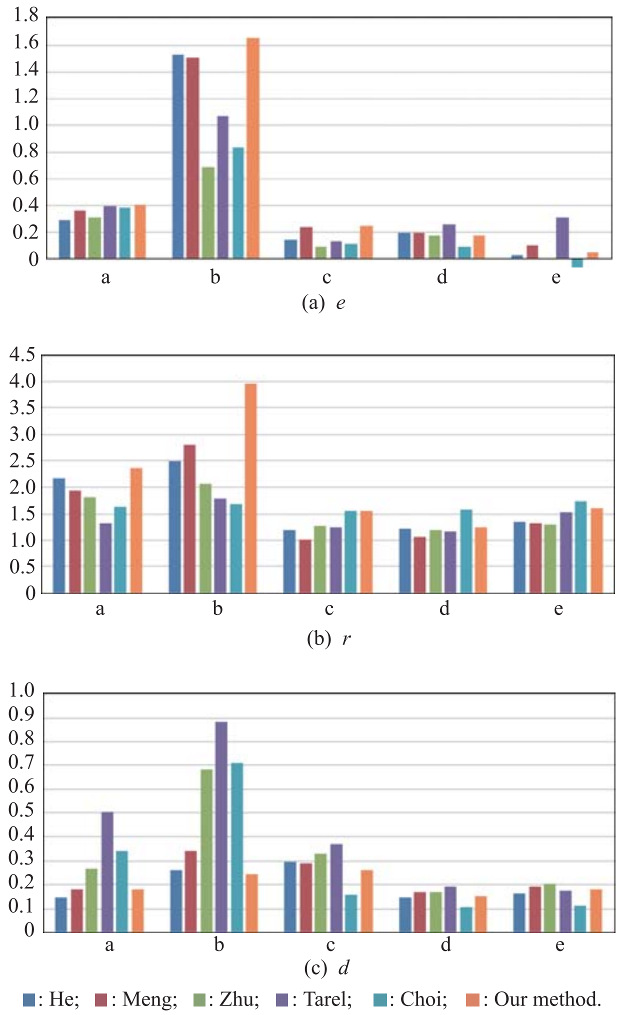

Fig. 6 Comparison results in terms of e, r, d

Table 1 Time consumption comparison s

Hazy image (resolution)	He [6]	Meng [9]	Zhu [16]	Choi [2]	Tarel [8]	Our method
Fig. 5(a) (173×139)	9.89	3.38	0.64	5.37	0.158	0.55
Fig. 5(b) (173×152)	10.20	3.15	0.43	3.88	0.179	0.54
Fig. 5(c) (173×130)	8.60	3.32	0.45	3.61	0.166	0.54
Fig. 5(d) (172×112)	7.51	2.84	0.43	3.13	0.132	0.53
Fig. 5(e) (173×260)	102.94	4.12	0.67	26.63	8.671	1.05

Table 1 lists the time consumption comparison with the other five algorithms. Evidently, our method has distinct speed advantages over He [6], Meng [9] and Choi [2]. However it consumes a bit more time than Zhu [16] and Tarel [8]. We also find that, Tarel [8] tends to be much slower in removing haze from images of large size. Although Zhu [16] achieves efficient processing even for large hazy images, its dehazing quality remains to be further improved.

6. Conclusions

In this paper, we propose a novel method to estimate the global atmospheric light by means of multiple priors found in input hazy images. Besides, an LP fusion process is presented to obtain a rough estimate of transmission map, which is further refined by an adaptive total variation model. To accelerate haze removal, we apply a fast iteration procedure to solve the TV model. Experiments demonstrate that our proposed method outperforms most state-of-the-art algorithms in terms of dehazing quality and computational efficiency.

Due to the dependency on dark channel prior, our method may share the common limitation with most of the DCP based algorithms. Our future work would focus on the improvement of the atmospheric scattering model, to solve the problem of haze removal in case of the inhomogenous atmosphere and uneven incident light.

References

[1] E. H. Land, J. J. Mccann. Lightness and retinex theory. *Journal of the Optical Society of America*, 1971, 61(1): 1 – 11.

[2] L. K. Choi, J. You, A. C. Bovik. Referenceless perceptual image defogging. *Proc. of the IEEE Southwest Symposium on Image Analysis and Interpretation*, 2014: 165 – 168.

[3] J. Kopf, B. Neubert, B. Chen, et al. Deep photo: model-based photograph enhancement and viewing. *ACM Trans. on Graphics*, 2010, 27(5): 32 – 39.

[4] Y. Y. Schechner, S. G. Narasimhan, S. K. Nayar. Instant dehazing of images using polarization. *Proc. of the IEEE Computer Society Conference on Computer Vision & Pattern Recognition*, 2001: 325 – 332.

[5] S. G. Narasimhan, S. K. Nayar. Contrast restoration of weather degraded images. *IEEE Trans. on Pattern Analysis & Machine Intelligence*, 2003, 25(6): 713 – 724.

[6] K. He, J. Sun, X. Tan. Single image haze removal using dark channel prior. *IEEE Trans. on Pattern Analysis & Machine Intelligence*, 2011, 33(12): 2341 – 2353.

[7] K. He, J. Sun, X. Tang. Guided image filtering. *IEEE Trans. on Pattern Analysis and Machine Intelligence*, 2013, 35(6): 1397 – 1409.

[8] J. P. Tarel, N. Hautiere. Fast visibility restoration from a single color or gray level image. *Proc. of the IEEE 12th International Conference on Computer Vision*, 2009: 2201 – 2208.

[9] G. Meng, Y. Wang, J. Duan, et al. Efficient image dehazing with boundary constraint and contextual regularization. *Proc. of the IEEE International Conference on Computer Vision*, 2013: 617 – 624.

[10] J. Zhang, S. Hu. A GPU-accelerated real-time single image de-hazing method using pixel-level optimal dehazing criterion. *Journal of Real-Time Image Processing*, 2014, 9(4): 661 – 672.

[11] R. T. Tan. Visibility in bad weather from a single image.

Proc. of the IEEE Conference on Computer Vision and Pattern Recognition, Anchorage, 2008: 1 – 8.

[12] J. H. Kim, W. D. Jang, J. Y. Sim, et al. Optimized contrast enhancement for real-time image and video dehazing. *Journal of Visual Communication & Image Representation*, 2013, 24(3): 410 – 425.

[13] J. B. Wang, N. He, L. L. Zhang, et al. Single image dehazing with a physical model and dark channel prior. *Neurocomputing*, 2015, 149(PB): 718 – 728.

[14] E. Namer, Y. Y. Schechner. Advanced visibility improvement based on polarization filtered images. *Proceedings of SPIE - The International Society for Optical Engineering*, 2005, 5888: 36 – 45.

[15] D. Nan, D. Y. Bi, S. P. Ma, et al. Single image dehazing method based on scene depth constraint. *Acta Electronica Sinica*, 2015, 43(3): 500 – 504. (in Chinese)

[16] Q. Zhu, J. Mai, L. Shao. A fast single image haze removal algorithm using color attenuation prior. *IEEE Trans. on Image Processing*, 2015, 24(11): 3522 – 3533.

[17] N. Hautière, J. P. Tarel, D. Aubert, et al. Blind contrast enhancement assessment by gradient ratioing at visible edges. *Image Analysis & Stereology*, 2008, 27(2): 87 – 95.

Biographies

Xuemei Wang was born in 1978. She received her B.S. degree from Changchun College of Posts and Telecommunications, China, in 2000 and M.S. degree from Nanjing University of Posts and Telecommunications, China, in 2003. Now, she is a lecturer and is working toward her Ph.D. degree in Nanjing University of Posts and Telecommunications, China. Her research interests mainly include image processing and computer vision.

E-mail: wangxm@njupt.edu.cn

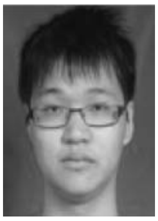

Mingye Ju was born in 1989. He received his B.S. degree in communication engineering from Nanjing University of Posts and Telecommunications, China, in 2010 and M.S. degree in signal and information processing from Tianjin University of Technology and Education, in 2013. Now, he is working toward his Ph.D. degree in information networks in Nanjing University of Posts and Telecommunications. His research interests mainly include image enhancement and image dehazing.

E-mail: 2014070245@njupt.edu.cn

Dengyin Zhang was born in 1964. He received his M.S. degree in circuit signal and system, and his Ph.D. degree in signal and information processing from Nanjing University of Posts and Telecommunications, Nanjing, China, in 1989, and 2004, respectively. He was elected as a master tutor and doctoral tutor in 2000 and 2010 respectively. His main research interests include signal and information processing, networking technique and information security.

E-mail: zhangdy@njupt.edu.cn